A&A 584, A55 (2015)
DOI: 10.1051/0004-6361/201527234

Astronomy & Astrophysics

On observing C_{60}^{+} and C_{60}^{2+} in laboratory and space

D. Strelnikov, B. Kern, and M. M. Kappes

Karlsruhe Institute of Technology, Institute of Physical Chemistry II, 76131 Karlsruhe, Germany
e-mail: dmitry.strelnikov@kit.edu

Received 24 August 2015 / Accepted 18 October 2015

ABSTRACT

Recently, we have measured the IR absorptions of C_{60}^{+}, C_{60}^{-}, and C_{60}^{2+} in neon matrixes. Many previously unknown absorptions were established. Here we compare our laboratory IR absorption spectra for C_{60}^{+} and C_{60}^{2+} to the IR emission spectra of several astronomical objects that show C_{60} emission. We find that IR bands of C_{60}^{+} are possibly present in the objects Tc1, SMP SMC 16, NGC 7023, NGC 2244, and SMP LMC 02. Infrared emission features possibly due to C_{60}^{2+} were identified in NGC 7023. To help with future observations of fullerene-related DIBs, we also revisited the oscillator strengths of the NIR absorptions of C_{60}^{+}, and report significantly revised values. Additionally, we report the UV oscillator strengths of C_{60}^{+}.

Key words. astrochemistry – molecular data – line: identification – methods: laboratory: molecular – planetary nebulae: general – infrared: planetary systems

1. Introduction

The unequivocal detection of neutral fullerenes C_{60} and C_{70} in the planetary nebula Tc1 in 2010 (Cami et al. 2010) has rekindled interest in fullerenes in space. Fullerenes (primarily C_{60}) have since been detected in several other astronomical objects (Otsuka et al. 2013; Iglesias-Groth & Esposito 2013; Sloan et al. 2014, and references therein). These observations are based on comparison of infrared (IR) emission data typically from space telescopes to laboratory IR absorption (Krätschmer et al. 1990) and high-temperature emission spectra (Nemes et al. 1994) extrapolated to lower temperatures.

Prior to the report by Cami et al. (2010), two diffuse interstellar bands (DIBs) at 958 and 963 nm had already been attributed to C_{60}^{+} (Foing & Ehrenfreund 1994) based on near-infrared (NIR) electronic absorption measurements in cryogenic matrixes (Fulara et al. 1993). However, this assignment was initially disputed (Maier 1994; Jenniskens et al. 1997; Misawa et al. 2009). More recently, the same DIBs were observed in the IRAS01005+7910 protoplanetary nebula (Iglesias-Groth & Esposito 2013), which also shows C_{60} IR emission features (Zhang & Kwok 2011). Laboratory measurements in gas phase (Campbell et al. 2015) have now conclusively shown that C_{60}^{+} is indeed the carrier of 958 and 963 nm DIBs.

We have recently built a setup for spectroscopy of ions in cryogenic inert gas matrixes and have used it to investigate $C_{60}^{+/-}$ over a wider IR spectral range than before. Many unknown absorptions were uncovered (Kern et al. 2013). Furthermore, we have obtained first IR/NIR/UV spectra of $C_{60}^{2+/3+}$ (Kern et al. 2014). A preliminary version of our data, containing parts of the $C_{60}^{+/-}$ IR spectra, was presented at a conference in 2012 (Kern et al. 2012). On this basis, C_{60}^{+} was rapidly identified in both the Tc1 young planetary nebula (Strelnikov et al. 2012) and in the NGC 7023 reflection nebula (Berné et al. 2013). Here we revisit the IR identification of interstellar C_{60}^{+} now making use of the complete laboratory data set and comparing it to emission spectra from five astronomical objects showing C_{60} features. Additionally we provide new measurements, including cross sections of UV/NIR absorption features to help with future observations.

2. Experiment and observations

The IR and UV-NIR absorption spectra of $C_{60}^{+/-}$ (Kern et al. 2013) and $C_{60}^{2+/3+}$ (Kern et al. 2014) have been reported previously along with experimental procedures and data analysis methods. Briefly, samples were prepared through low-energy ion beam deposition into a cocondensed inert gas matrix doped with electron scavengers (CO_2, CCl_4) as necessary to vary the resulting fullerene charge state distributions. Two different electron scavengers were used to assure coverage of the full IR spectral region (free of overlap with electron scavenger absorptions). Here, we have extended these measurements to Ar matrixes.

We primarily compare the laboratory infrared spectra to astronomical data obtained from the *Spitzer* Heritage Archive: NGC 2244 (RA 06:31:48.05; Dec 04:19:36.6; AORKEY 25646080, 25646336; PI Jacqueline Keane), LMC02 (RA 04:40:56.78; Dec –67:48:01.2; AORKEY 4946944; PI James R. Houck), NGC 7023 (RA 21:01:41.95; Dec 68:09:50.7; AORKEY 23910912, 23911424; PI Kris Sellgren), SMC16 (RA 00:51:27.15; Dec –72:26:13.5; AORKEY 14706944; PI Letizia Stanghellini) and Tc1 (RA 17:45:35.08; Dec –46:05:22.7; AORKEY 11321600; PI Mathew Bobrowsky). Spectral data was extracted using the CUBISM program (Smith et al. 2007). The dust continuum background was subtracted as in Cami et al. (2010).

3. Results

3.1. Laboratory IR data

The experimental procedure and in particular the methods used to deconvolute the superimposed $C_{60}^{0/+/-}$ absorption spectra have

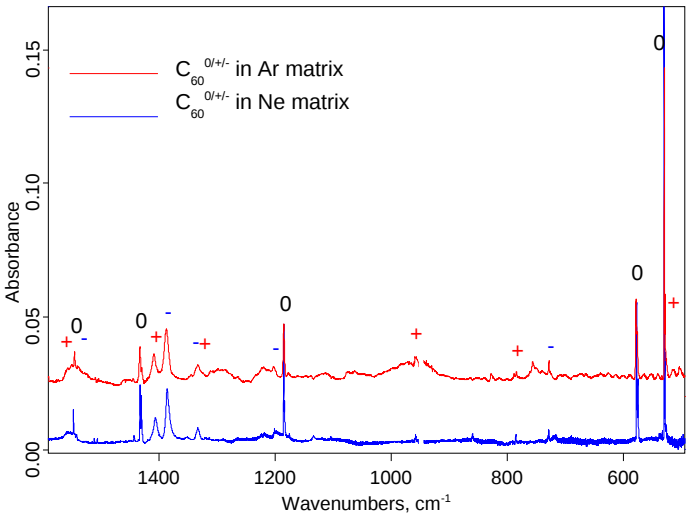

Fig. 1. Infrared spectra of $C_{60}^{0/+/-}$ in Ne and Ar matrixes over the range 500–1590 cm^{-1}. Absorptions of different C_{60} charge states are indicated with 0, + and – for neutral, cation, and anion, respectively.

been described in detail in our previous work (Kern et al. 2013, 2014). IR frequencies of C_{60}, C_{60}^+, and C_{60}^- absorptions in Ne and Ar matrixes are presented in Table 1 together with Ne data for C_{60}^{2+}. Overview spectra for C_{60}, C_{60}^+, and C_{60}^{2+} can be found in Fig. 1. Since there are no gas-phase IR absorption or emission measurements for $C_{60}^{+/2+}$ so far, we estimate the low-temperature gas-phase absorption frequencies from the matrix data. It is known, that Gas-Ne matrix IR frequency shifts are in general smaller than Gas-Ar shifts (Jacox 1994). The primary reason is the lower polarizability of solid Ne and hence the weaker interaction of an oscillating dipole with its environment. In analogy to a damped oscillator, the Ne environment would have a lower damping coefficient in comparison to an Ar environment. If both Ne and Ar vibrational frequencies are close to each other – as is the case here – this implies that interaction with the matrix does not significantly influence an unperturbed vacuum vibration. Similar ideas were used to estimate the gas-phase electronic absorption frequency of C_{60}^+ from frequencies of complexes C_{60}^+·He, and C_{60}^+·He_2 (Campbell et al. 2015). For C_{60} ions, only small changes of absorption frequencies occur upon switching from Ne to Ar. Therefore, gas phase absorptions of $C_{60}^{+/2+}$ at 5 K should be close to absorptions in matrix. Matrix absorption frequencies can be extrapolated to a gas-phase environment with zero polarizability ($\alpha_{Gas} = 0$) by assuming $\nu_{Gas} - \nu_{Matrix} \sim \alpha_{Matrix}$; see Table 1. For large molecules like fullerenes, matrix site effects should not significantly affect the vibrational potential surfaces.

3.2. Laboratory UV-NIR data

Our data on NIR absorptions of $C_{60}^{+/-}$ are very similar to Fulara et al. (1993) with the only difference being that the oscillator strengths are significantly larger. On the basis of integrated molar absorptivities previously measured for $C_{60}^{+/-}$ in the IR region (Kern et al. 2013), the C_{60}^+ NIR oscillator strengths are determined as $f = 0.015 \pm 0.005$ for the 966 nm and $f = 0.01 \pm 0.003$ for the 958 nm absorptions (see Fig. 2). It remains to be understood why the intensity ratio of the two strongest C_{60}^+ NIR absorptions in Ne matrix ($I_{966}/I_{958} = 1.5$) differs from the recently published (Campbell et al. 2015) gas-phase NIR spectrum of C_{60}^+·He ($I_{963}/I_{958} = 0.8$). The oscillator strength of the C_{60}^- absorption at 1058 nm is 0.022 ± 0.005.

C_{60}, C_{60}^+, C_{60}^- and C_{60}^{2+} all have very similar UV absorption features with minimal spectral shifts (Kern et al. 2014). Figure 3 shows corresponding UV-NIR spectra of two different $C_{60}^+/C_{60}^-/C_{60}$ mixtures in Ne+1% CO_2 (B) and Ne matrixes (A). We scaled spectra A and B to the same absorbance of neutral C_{60} in the characteristic 600 nm range and then subtracted spectrum A, with less C_{60}^+ , from spectrum B, with much more C_{60}^+ (CO_2 electron scavenger doping prevents neutralization of soft-landed C_{60}^+). This procedure removes all C_{60} contributions such that essentially all absorption features remaining are due to C_{60}^+ (an estimated amount of C_{60}^- is ≤4%). To obtain a C_{60}^+ spectrum, one does not need information about the relative abundances of $C_{60}^{0/+/-}$ in the samples. These compositions can however be estimated from known IR absorptivity data (Kern et al. 2013). Sample A contains approximately 74/13/13 of $C_{60}^+/C_{60}^-/C_{60}$, while the relative ratio in the sample B is estimated to be about 24/72/4. In Fig. 3, strong C_{60}^+ transitions at 322 and 960 nm are indicated with arrows. The oscillator strength of the 322 nm band, as calibrated against the 960 nm band, is 0.3 ± 0.15, which is close to the value of 0.37 for the corresponding C_{60} band (Sassara et al. 2001). Increasing light scattering further to the UV precludes estimating cross sections of higher energy C_{60}^+ bands. Nevertheless, their intensities are comparable to those of C_{60}.

3.3. Comparison to astronomical observations

Before comparing laboratory IR absorption to astronomical emission data one should first consider possible systematic differences in the peak positions and line intensities.

Frequencies. The matrix environment can influence IR frequencies inducing both blue- or redshifts relative to low temperature measurements in gas phase. Our Ne and Ar matrix data (Table 1) indicate that such shifts are small here. Bigger shifts could result from different vibrational excitation levels in gas phase vs. matrix. Nemes et al. (1994) observed that IR emission bands of C_{60} shift to lower frequencies with increasing temperature, reflecting anharmonicity. Correspondingly, the differences between matrix absorption and gas-phase emission frequencies increase. In fact, small redshifts of transitions at 7.0 and 8.5 μm have been observed in comparing laboratory and astronomical data (García-Hernández et al. 2010), especially for the 8.5 μm C_{60} emission. We do not expect significantly larger redshifts for $C_{60}^{+/2+}$ and, therefore, do not correct the laboratory frequencies.

Intensities. Two different approaches have been used to compare laboratory C_{60} IR absorption intensities to astronomical emission data: (i) modulation of line strengths to reflect thermal equilibrium with the surroundings (Cami et al. 2010); or (ii) simulation of IR emission for vibrationally excited species, as generated by UV absorption followed by radiationless relaxation into the ground electronic state (Sellgren et al. 2010). Qualitatively, for both approaches, the higher the emission temperatures the (relatively) weaker the long wavelength bands become. By contrast, a comparison of cryogenic matrix absorption with gas-phase emission data for pyrene cations illustrates that the associated effects may not always be large enough to require a correction (Kim & Saykally 2003)

With above caveats in mind, we have examined emission spectra of many astronomical objects in which C_{60} has been observed. In several cases we have found candidate features resembling C_{60}^+ and C_{60}^{2+} IR absorption spectral patterns.

Table 1. $C_{60}^{0/+/-}$ absorption frequencies ν (in cm^{-1}) in different environments, Ne, Ar matrixes, and gas phase at 5 K, and corresponding integrated molar absorptivity in Ne A_{Ne} (in km mol^{-1}).

	Mode	ν_{Ne} [b] (cm^{-1})	ν_{Ar} [b] (cm^{-1})	ν_{Gas} (cm^{-1})	A_{Ne} (km·mol^{-1})
C_{60}^{0}	comb.[a]	1547.0	1545	1547.6	2 ± 0.2
C_{60}^{0}	$T_{1u}(4)$	*1432.1;* 1430.1	*1432.5;* 1429.3	1431	11 ± 1
C_{60}^{0}	$T_{1u}(3)$	1184.8	1184.9	1184.8	10.4 ± 0.8
C_{60}^{0}	$T_{1u}(2)$	577.8	578.8	577.5	11 ± 0.9
C_{60}^{0}	$T_{1u}(1)$	530.4	529.8	530.6	27 ± 2
C_{60}^{+}	$E_{1u}(17)$	1557.6	1558.1	1557.4	33 ± 9
C_{60}^{+}	$E_{1u}(15)$	1405.3	1408.3	1404.4	70 ± 19
C_{60}^{+}	$E_{1u}(14)$	1331.1	1331.5	1331.0	20 ± 5
C_{60}^{+}	$A_{2u}(7)$	1223.2	1223.2	1223.2	6 ± 2
C_{60}^{+}	$E_{1u}(12)$	1218.1	1219.1	1217.8	11 ± 3
C_{60}^{+}	$E_{1u}(10)$	958.2	958.2	958.2	4 ± 1
C_{60}^{+}	$E_{1u}(7)$	785.7	784.8	786.0	4 ± 1
C_{60}^{+}	$E_{1u}(5)$	580.0	unclear		1.6 ± 1
C_{60}^{+}	$A_{2u}(2)$	529.7	unclear		20 ± 5
C_{60}^{+}	$E_{1u}(3)$	526.6	526.3	527.7	7 ± 2
C_{60}^{+}	$E_{1u}(2)$	*398.5*; 395.0	*398.3*; 395.1	*398.6*; 395.0	10 ± 3
C_{60}^{+}	$E_{1u}(1)$	347.2	348.1	346.9	5 ± 2
C_{60}^{-}	$E_{u}(28)$	1546.1	1542.2	1547.3	16 ± 4
C_{60}^{-}	$E_{u}(25)$	1385.5	1386.9	1385.1	128 ± 14
C_{60}^{-}	$E_{u}(24)$	1351.6	1344.2	1353.9	5 ± 1.5
C_{60}^{-}	$E_{u}(23)$	1333.6	1334.8	1333.2	8 ± 3
C_{60}^{-}	$E_{u}(19)$	1200.7	1202.5	1200.1	16 ± 4
C_{60}^{-}	$A_{2u}(10)$	1175.6	1176.5	1175.3	1.3 ± 0.5
C_{60}^{-}	$E_{u}(17)$	964.3	unclear		0.9 ± 0.4
C_{60}^{-}	$E_{u}(11)$	729.2	728.5	729.4	6 ± 2
C_{60}^{-}	$A_{2u}(4)$	576.4	577.8	576.0	8 ± 3
C_{60}^{-}	$E_{u}(8)$	575.3	576.6	574.9	39 ± 4
C_{60}^{-}	$E_{u}(3)$	397.2	397.3	397.2	0.8 ± 0.3
C_{60}^{2+}	$E_{1u}(17)$,	1565.5			45 ± 18
C_{60}^{2+}	$A_{2u}(9)$	*1562.1*; 1559.9			25.5 ± 10
		1556.7; 1552.5			
C_{60}^{2+}	$E_{1u}(15)$	*1396.4*			50 ± 20
C_{60}^{2+}	$E_{1u}(14)$	1323.1; 1322.6			8 ± 3
		1320.6			
C_{60}^{2+}	$E_{1u}(13)$	1307.3; 1304.8			12 ± 5
		1302.7			
C_{60}^{2+}	$A_{2u}(7)$	*1278.3*; 1275.2			11 ± 4
C_{60}^{2+}	$E_{1u}(12)$	*1232.3*; 1230.6			7 ± 3
		1228.5			
C_{60}^{2+}	$E_{1u}(11)$	1168.9			1 ± 0.5
C_{60}^{2+}	$A_{2u}(5)$	*974.1*; 972.7			5 ± 2
C_{60}^{2+}	$E_{1u}(10)$	*952.9*; 951.7			8 ± 3
C_{60}^{2+}	$A_{2u}(2)$,	*525.7*			2 ± 1

Notes. Gas-phase values were obtained by extrapolation of matrix data (see main text, Sect. 3.1). In several cases, IR absorption features of C_{60}^{+} in Ar matrix (increased FWHM relative to Ne matrix) could not be clearly distinguished from overlapping C_{60} absorptions. These cases are designated as unclear. [(a)] Combination mode. [(b)] Multiple absorption lines are due to multiple site effects or other matrix distortions; the most intense line is in italics.

C_{60}^{+}. Figures 4 and 5 contrast IR emission spectra (5.2–11 μm, 11–35 μm) for the objects Tc1, SMP SMC 16, NGC 7023, NGC 2244, and SMP LMC 02 with laboratory IR absorption spectra in Ne matrix. A dust continuum background has been subtracted from the astronomical spectra as in Cami et al. (2010). The red dashed vertical lines with plus signs indicate possible features of C_{60}^{+} whereas blue dashed lines with double plus signs indicate possible features of C_{60}^{2+}. We

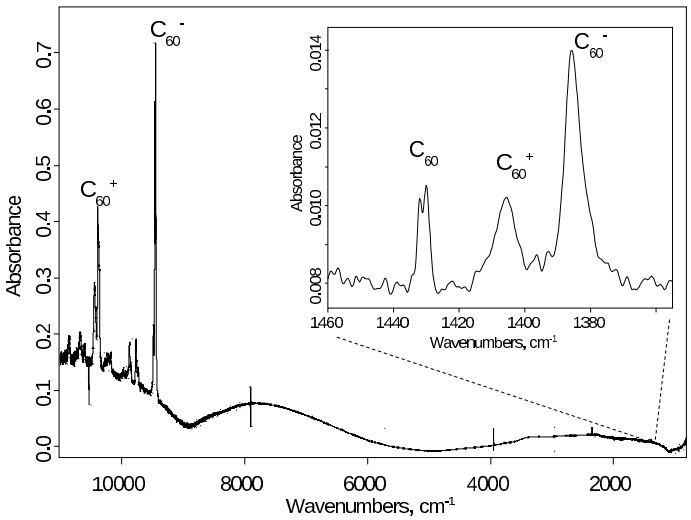

Fig. 2. Absorption spectrum obtained for a sample of Ne matrix isolated $C_{60}^{0/+/-}$ over the complete NIR and IR spectral range using a halogen/Globar light source and a broadband MCT detector. Shown in the *inset* is a 60x expanded scale representation of a segment of the IR spectrum, containing absorption features assigned to C_{60}, C_{60}^{+} and C_{60}^{-}, respectively.

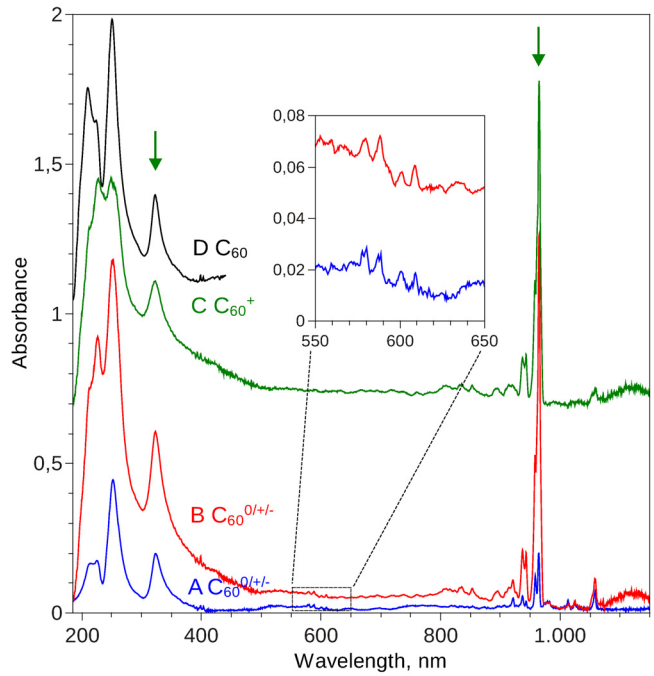

Fig. 3. UV-NIR absorption spectra recorded for matrixes with two different charge state ratios of $C_{60}^{0/+/-}$. A: $C_{60}^{0/+/-}$ in Ne matrix. B: $C_{60}^{0/+/-}$ in Ne+1% CO_2 matrix. B comprises much more C_{60}^{+} than A. The *inset* shows weak absorptions of C_{60}. C shows the difference spectrum resulting from subtraction of A from B. D shows the reference UV spectrum of neutral C_{60} in Ne+1% CO2 matrix.

multiplied the absorbance of the C_{60} laboratory spectrum by a Planck distribution for T = 330 K and then scaled to the 17.4 and 18.9 μm bands of C_{60} in Tc1, following the procedure used by Cami et al. (2010).

A band at 6.48 μm is present in all astronomical spectra. This was previously assigned to a hydrogen recombination line by Cami et al. (2010), however, there is no such 6.48 μm line in the NIST atomic spectral database (NIST 2013) and no other published evidence for it. We suggest, therefore, that hydrogen is not responsible and instead assign the feature to the $E_{1u}(17)$ C_{60}^{+} infrared vibration. Sloan et al. (2014) also recently designated a 6.5 μm band observed in several Magellanic Cloud objects as fullerene related. The intensities of astronomical and laboratory spectra in the Figs. 4 and 5 were scaled to have comparable strengths at the purported 6.48 μm absorption/emission line of C_{60}^{+} for easier comparison of possible $C_{60}^{+/2+}$ features. The red dashed curve indicates the effect of applying the same 330 K intensity modulation to the unmodulated C_{60}^{+} spectrum (solid red line). The intensities of the modulated C_{60}^{+} spectrum have been scaled to fit the intensities of the unmodulated spectrum in the 5.2–11 μm region.

We searched for additional C_{60}^{+} features by comparing experimental and laboratory data sets further to the red. The band observed in the laboratory spectrum at about 7.11 μm ($E_{1u}(15)$ C_{60}^{+}) appears to be occluded by strong overlapping ArII and C_{60} neutral emissions, in particular, in the Tc1 spectrum. It can be better distinguished in the other objects in Fig. 4. The hydrogen recombination bands at 7.46 and 7.5 μm (NIST 2013) mask the C_{60}^{+} feature there. Referring next to Fig. 4, more or less pronounced emission features are always present in the vicinity of the 8.2 μm C_{60}^{+} band. The line at 10.45 μm ($E_{1u}(10)$ C_{60}^{+}) can be distinguished in the high-resolution SH data for Tc1 and, possibly, for NGC 2244. The line at about 12.8 μm ($E_{1u}(7)$ C_{60}^{+}) appears occluded by strong NeII emission. To longer wavelengths, the C_{60}^{+} IR absorption spectrum possesses two features at 17.4 and 18.9 μm that are not clearly resolvable from those of C_{60}. Additionally, two characteristic C_{60}^{+} absorption bands are seen at 25.3 and 28.8 μm. The latter bands cannot be distinguished in the low-resolution LL data. However, a band at 28.9 μm in the high-resolution LH data of Tc1 may correspond to the $E_{1u}(1)$ C_{60}^{+} vibration. At the same time, there is no clear candidate for the 25.3 μm $E_{1u}(2)$ C_{60}^{+} band. An additional complication arises from interferences due to the IR detector of the IRAS instrument in this emission wavelength range. One way to overcome the problem of missing/unclear 25.3 and 28.8 μm C_{60}^{+} emissions is to assume that the relative intensities of these long wavelength bands are lowered by high emission temperatures.

Fullerene and mixed spectra for several objects in the Magellanic Clouds (Sloan et al. 2014) show the 17.4 and 18.9 C_{60} bands with a wide range of intensity ratios. This was ascribed to superimposed 18.71 μm SIII emission, but it may instead reflect different relative contributions of the stronger 18.9 μm feature of C_{60}^{+} (see Fig. 5).

C_{60}^{2+} . The laboratory IR absorption data obtained for C_{60}^{+} and C_{60}^{2+} are similar in the short wavelength region. Nevertheless, the presence of C_{60}^{2+} should be indentifiable by two characteristic emissions shifted somewhat to the blue and to the red of the C_{60}^{+} 6.48 and 7.11 features, respectively. The features at 6.42 and at 7.16 μm in the NGC 7023 object, and possibly also in NGC 2244 and SMP LMC 02 may correspond to C_{60}^{2+}. Further C_{60}^{2+} absorption features are either hidden by broad PAH emission bands or are too weak to be distinguished.

4. Discussion

4.1. Characteristic IR emission features

Infrared absorptions of C_{60}^{+} in Ne and Ar matrixes at 5 K are very similar and should therefore also be close to the low-temperature gas-phase absorption frequencies of C_{60}^{+}; see Sect. 3.1. By

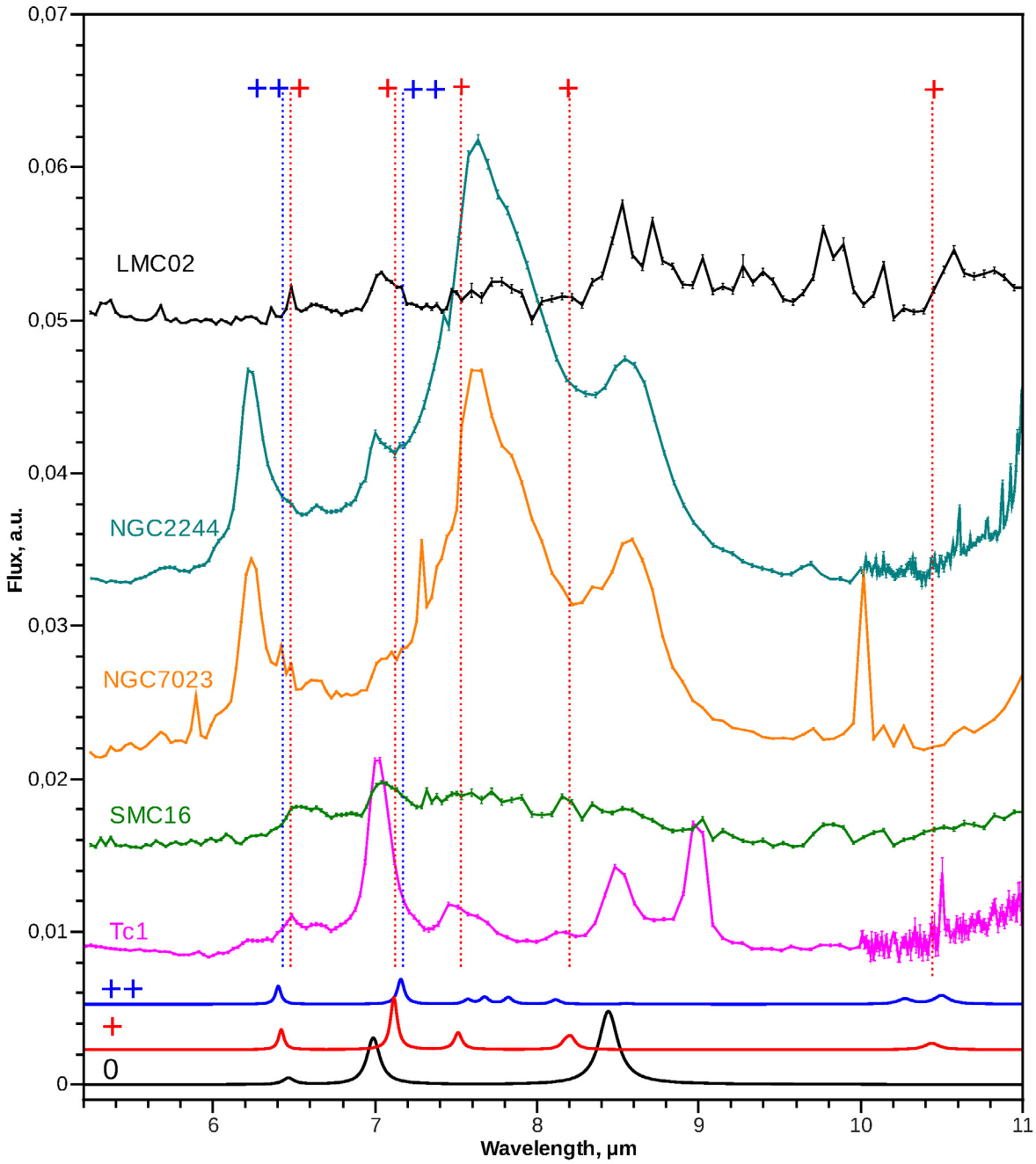

Fig. 4. IR emission *Spitzer* data of various astronomical objects vs. laboratory absorptions of C_{60} (black), C_{60}^{+} (red), and C_{60}^{2+} (blue) (broadened by Lorentz functions with 10 cm^{-1} fwhm for $C_{60}^{+/2+}$ and 20 cm^{-1} fwhm for neutral C_{60}).

contrast, the absorption frequencies of C_{60}, C_{60}^{+} C_{60}^{2+} differ considerably, particularly in the 5.5–10 μm wavelength range. Thus, C_{60}, C_{60}^{+}, and C_{60}^{2+} should be distinguishable from one another on the basis of their gas-phase IR emission spectra.

A comparison of IR emission spectra of C_{60}-containing objects with laboratory absorption data for $C_{60}^{+/2+}$ tentatively reveals the presence of C_{60}^{+}, and possibly also C_{60}^{2+}, in the five astronomical objects. As they would likely be neutralized if embedded in dust particles, the cations must be isolated in gas phase. Another reason for invoking a gas-phase environment is the observation of IR emission bands. The main relaxation channel for large cationic species in gas phase would be IR emission, while for possibly embedded ions, relaxation would be expected to primarily proceed through phonon exchange with the environment: no fullerene specific IR emission features would be observed. Two mechanisms could be responsible for the ionization of C_{60}: UV photoionization and/or cosmic-ray induced ionization. The first, second, and third ionization energies of C_{60} are 7.6 eV, 11.4 eV and 16.6 eV, respectively (Wörgötter et al. 1994). Further discussion on ionization mechanisms goes beyond the scope of this study.

Based on our preliminary laboratory IR absorption data, C_{60}^{+} had already been tentatively identified in NGC 7023 ("Position 2") using IR emission lines observed at 6.43, 7.13, 8.1, and 10.53 μm (Berné et al. 2013). This differs only slightly from our preferred assignment of emission features observed at 6.48, 7.14, 8.2, and 10.45 μm to C_{60}^{+} on the basis of the complete laboratory data set and in comparison

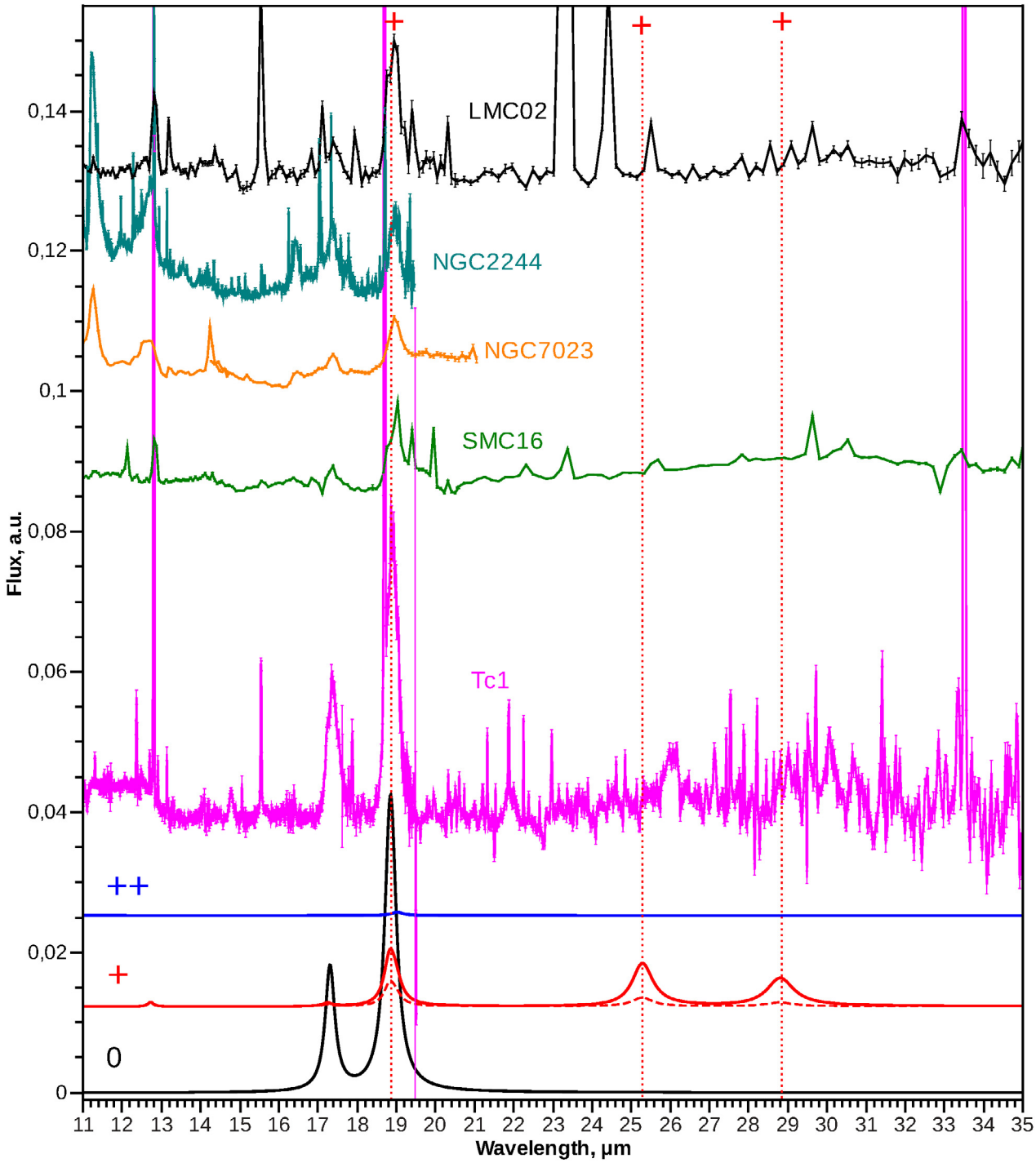

Fig. 5. IR emission *Spitzer* data of various astronomical objects vs. laboratory absorptions of C_{60} (black), C_{60}^{+} (red solid and dashed), and C_{60}^{2+} (blue) (broadened by Lorentz functions with 10 cm^{-1} fwhm (20 cm^{-1} fwhm for neutral C_{60})).

to observations for four more objects (Tc1, SMP SMC 16, NGC 2244, and SMP LMC 02). Nevertheless, these assignments remain tentative until higher resolution astronomical data become available in particular in the 5–10 μm region.

4.2. Relative abundances

Estimating C_{60}^{+}/C_{60} abundance ratios depends on assumptions concerning temperature-dependent modulations of infrared emission intensities. If a Planck's law modulation with T = 330 K is applied to both C_{60}^{+} and C_{60} laboratory data sets (Cami et al. 2010), the Tc1 emission spectrum is best described by a C_{60}^{+}/C_{60} ratio of 1:10. A more qualitative way to estimate the abundance ratio C_{60}^{+}/C_{60} is to compare the intensities of the 8.5 and 7.0 μm C_{60} features with those of the 6.48 and 7.14 μm bands of C_{60}^{+}. As the relative strengths and positions of these bands are similar, modulation of IR emission intensities does not significantly influence the ratios. The SMP SMC 16 spectrum has a quite weak 8.5 μm C_{60} band and a weak 7.0 μm ArII/C_{60} band, whereas the rest of the spectrum is very similar to that of Tc1. Therefore most of the intensity flux at 6.48 and 7.14 μm and a considerable part of the 18.9 μm

emission is due to C_{60}^+, i.e., C_{60}^+ is more abundant than C_{60}. Determination of fullerene charge state ratios in NGC 7023 and NGC 2244 is complicated by strong PAH emission features at 6.2 and 8.6 μm, which partially occlude the 6.48 μm C_{60}^+ and 8.5 μm C_{60} bands. Nevertheless, given that the relative intensities of 6.48, 17.4, and 18.9 μm features are roughly similar in NGC 7023, NGC 2244, and SMP SMC 16, similar C_{60}^+/C_{60} ratios can be inferred. If C_{60}^{2+} is present in NGC 7023 its abundance would be about 50% of that of C_{60}^+.

4.3. Fullerene related DIBs

The recent conclusive assignment of DIBs at 958 and 963 nm to NIR absorptions of C_{60}^+ (Campbell et al. 2015) has already been mentioned. We find the corresponding oscillator strengths ($f = 0.015 \pm 0.005$ for the 966 nm absorption and $f = 0.01 \pm 0.003$ for the 958 nm absorption) to be significantly larger than previously reported. On the basis of our tentative identification of C_{60}^+ in the IR emission of the objects considered here, we also recommend looking for their 958 and 963 nm DIBs. So far, C_{60}^+ DIBs have only been seen in one C_{60} containing object, IRAS01005+7910, (Iglesias-Groth & Esposito 2013). However, this shows no clear IR signatures of C_{60}^+, as has been already pointed out (Dìaz-Luis et al. 2015).

C_{60}^+ also has several strong UV absorptions (Fig. 3). Whereas NIR signatures are characteristic, and the UV absorptions of different fullerene charge states are calculated (and partly measured) to be quite similar, particularly when considering line broadening (Kern et al. 2014). Nevertheless, if NIR absorptions of C_{60}^+ are present, then strong UV absorptions near 320 and 250 nm must also be detectable. Future work on fullerene related DIBs should also take the UV spectral region into account. So far, there has been no clear astronomical observation of C_{60} in the UV (Herbig 2000).

Concerning higher charge states, C_{60}^{2+} has no strong NIR features, but C_{60}^{3+} again has specific NIR absorptions in Ne at 899 and 857 nm (Kern et al. 2014). Based on the IR data of $C_{60}^{+/2+}$ and $CCl_3{\cdot}Cl^-$ counter-ion absorptions, we estimate the oscillator strengths of these two absorptions as $f = 0.002 \pm 0.001$ and $f = 0.0004 \pm 0.0002$, respectively. No other laboratory spectroscopic data for C_{60}^{3+} exists so far. We recommend bands close to 899 and 857 nm as candidate bands for future astronomical surveys.

5. Conclusions

Infrared absorptions of C_{60}^+ and C_{60}^{2+} in inert gas matrixes have been compared to the IR emission spectra of several astronomical objects showing C_{60} emission. We find that C_{60}^+ may be present in the objects Tc1, SMP SMC 16, NGC 7023, NGC 2244, SMP LMC02. In addition, C_{60}^{2+} is possibly present in NGC 7023. Higher resolution astronomical data in the 5–10 μm region would significantly improve the reliability of future IR observations of $C_{60}^{0/+/2+}$.

To help with future observations of fullerene-related DIBs, we also revisited the oscillator strengths of the electronic NIR absorptions of C_{60}^+ and report significantly revised laboratory values. We provide two candidate NIR bands for future astronomical surveys of C_{60}^{3+}. Finally, we recommend that the UV region should also be considered in future astronomical observations of $C_{60}^{0/+/-/2+}$.

Acknowledgements. This work was supported by the Deutsche Forschungsgemeinschaft (KA 972/10-1). We thank W. Krätschmer (Max-Planck Institute for Nuclear Physics) for helpful discussions.

References

Berné, O., Mulas, G., & Joblin, C. 2013, A&A, 550, L4
Cami, J., Bernard-Salas, J., Peeters, E., & Malek, S. 2010, Science, 329, 1180
Campbell, E. K., Holz, M., Gerlich, D., & Maier, J. P. 2015, Nature, 523, 322
Dìaz-Luis, J. J., Garcìa-Hernàndez, D. A., Rao, N. K., Manchado, A., & Cataldo, F. 2015, A&A, 573, A97
Foing, B. H., & Ehrenfreund, P. 1994, Nature, 369, 296
Fulara, J., Jakobi, M., & Maier, J. 1993, Chem. Phys. Lett., 211, 227
García-Hernández, D., Manchado, A., García-Lario, P., et al. 2010, ApJ, 724, L39
Herbig, G. H. 2000, ApJ, 542, 334
Iglesias-Groth, S., & Esposito, M. 2013, ApJ, 776, L2
Jacox, M. E. 1994, Chem. Phys., 189, 149
Jenniskens, P., Mulas, G., Porceddu, I., & Benvenuti, P. 1997, A&A, 327, 337
Kern, B., Strelnikov, D., Weis, P., Böttcher, A., & Kappes, M. M. 2012, C_{60}^+ and C_{60}^- in Neon Matrices and Argon Matrices, 68th Int. Symp. on Molecular Spectroscopy, https://molspect.chemistry.ohio-state.edu/symposium_67/symposium/Program/MJ.html#MJ08
Kern, B., Strelnikov, D., Weis, P., Böttcher, A., & Kappes, M. M. 2013, J. Phys. Chem. A, 117, 8251
Kern, B., Strelnikov, D., Weis, P., Böttcher, A., & Kappes, M. M. 2014, J. Phys. Chem. Lett., 457
Kim, H.-S., & Saykally, R. J. 2003, Rev. Sci. Instrum., 74, 2488
Kramida, A., Ralchenko, Y., & Reader, J. 2014, NIST Atomic Spectra Database (version 5.1), Online, Available: http://physics.nist.gov/asd, National Institute of Standards and Technology, Gaithersburg, MD
Krätschmer, W., Lamb, L., Fostiropoulos, K., & Huffman., D. 1990, Nature, 347, 354
Maier, J. P. 1994, Nature, 370, 423
Misawa, T., Gandhi, P., Hida, A., Tamagawa, T., & Yamaguchi, T. 2009, ApJ, 700, 1988
Nemes, L., Ram, R. S., Bernath, P. F., et al. 1994, Chem. Phys. Lett., 218, 295
Otsuka, M., Kemper, F., Hyung, S., et al. 2013, ApJ, 764, 77
Sassara, A., Zerza, G., Chergui, M., & Leach, S. 2001, ApJS, 135, 263
Sellgren, K., Werner, M. W., Ingalls, J. G., et al. 2010, ApJ, 722, L54
Sloan, G. C., Lagadec, E., Zijlstra, A. A., et al. 2014, ApJ, 791, 28
Smith, J. D. T., Armus, L., Dale, D. A., et al. 2007, PASP, 119, 1133
Strelnikov, D., Kern, B., Böttcher, A., & Kappes, M. M. 2012, Laboratory and Space Infrared Detection of C_{60}^+, PRAHA2012, the 22nd Int. Conf. on High Resolution Molecular Spectroscopy
Wörgötter, R., Dünser, B., Scheier, P., & Märk, T. D. 1994, J. Chem. Phys., 101, 8674
Zhang, Y., & Kwok, S. 2011, ApJ, 730, 126